Title

Electron-phonon interaction and thermal boundary resistance at the crystal-amorphous interface of the phase change compound GeTe

Journal

Journal of Applied Physics, 117(1)

ISSN

0021-8979

Authors

Campi, Davide
Donadio, Davide
Sosso, Gabriele C
et al.

Publication Date

2015-01-07

DOI

10.1063/1.4904910

Peer reviewed

Electron-phonon interaction and thermal boundary resistance at the crystal-amorphous interface of the phase change compound GeTe.

Davide Campi[1], Davide Donadio[2], Gabriele C. Sosso[1,3], Jörg Behler[4], and Marco Bernasconi[1*]
[1] *Dipartimento di Scienza dei Materiali, Università di Milano-Bicocca, Via R. Cozzi 53, I-20125, Milano, Italy*
[2] *Max Planck Institute for Polymer Research, Ackermannweg 10, D-55128 Mainz, Germany*
[3] *Computational Science, Department of Chemistry and Applied Biosciences, ETH Zurich, USI Campus, via Giuseppe Buffi 13, CH-6900 Lugano, Switzerland and*
[4] *Lehrstuhl für Theoretische Chemie, Ruhr-Universität Bochum, Universitätsstrasse 150, D-44780 Bochum, Germany*

Phonon dispersion relations and electron-phonon coupling of hole-doped trigonal GeTe have been computed by density functional perturbation theory. This compound is a prototypical phase change materials of interest for applications in phase change non-volatile memories. The calculations allowed us to estimate the electron-phonon contribution to the thermal boundary resistance at the interface between the crystalline and amorphous phases present in the device. The lattice contribution to the thermal boundary resistance has been computed by non-equilibrium molecular dynamics simulations with an interatomic potential based on a neural network scheme. The electron-phonon term contributes to the thermal boundary resistance to an extent which is strongly dependent on the holes concentration and mobility. For measured values of the holes concentration and electrical conductivity the electron-phonon term overcomes the contribution from the lattice to the thermal boundary resistance. It is also shown that the presence of Ge vacancies, responsible for the p-type degenerate character of the semiconductor, strongly affect the lattice thermal conductivity of the crystal.

I. INTRODUCTION

Chalcogenide alloys are attracting an increasing interest for their use in optical data storage (digital versatile disk, DVD) and, more recently, in electronic non volatile memories (Phase Change Memories, PCM)[1–5]. These applications rest on a fast and reversible transformation between the amorphous and crystalline phases upon heating. The two phases can be discriminated thanks to a large contrast in their electrical conductivity (in PCM) and optical reflectivity (in DVD). In PCM operation, cell read-out is performed at low bias. Programming the memory requires instead a relatively large current to heat up the active layer and induce the phase change: either the melting of the crystal and subsequent amorphization or the recrystallization of the amorphous.

Thermal conductivity (κ) is a key property for the device operation, as the set/reset processes strongly depend upon heat dissipation and transport. In particular, the thermal boundary resistance (TBR) with the surrounding dielectrics are crucial parameters for the control of thermal cross-talks with adjacent cells which may arise during memory programming. A large TBR can also lead to a reduction in the programming current thanks to heat confinement effects[6]. The complete electrothermal modeling of PCM operation thus requires the knowledge of the TBR at different interfaces which are often difficult to be measured accurately at the operation conditions of the PCM cells. Since the amorphous region is embedded in a crystalline, untransformed matrix, the junction between the crystal and the amorphous region is one of the interfaces expected to mainly affect the operation of PCM devices.

Atomistic simulations can provide crucial insights into the thermal transport properties of phase change materials, suitable to aid a reliable modeling of the device operation. Simulations based on density functional theory (DFT) have indeed provided detailed information on several features of phase change materials in the last few years (see for example Refs.[7–10]). However, the calculation of the thermal conductivity in an amorphous system and at its interface with the crystal requires very long simulations of large models, which are presently beyond the reach of fully DFT simulations. To overcome these limitations, we have recently developed an interatomic potential for the GeTe phase change compound[11], by fitting a large database of DFT energies by means of the Neural Network (NN) method introduced by Behler and Parrinello[12]. The potential displays an accuracy close to that of the underlying DFT framework in describing the structural and dynamical properties of GeTe.

In this paper, we report on the calculation of the TBR at the crystal/amorphous interface of GeTe phase change compound. Although the ternary system $Ge_2Sb_2Te_5$ (GST) is mostly studied for PCM applications, the binary GeTe compound is also under scrutiny for applications[13] as it shares most of the properties with the more commonly used GST. We expect the presence of both electronic and lattice contributions to the TBR. The lattice contribution stems from the mismatch in the vibrational modes of the two phases. In fact the phonons of the amorphous phase display a softening in the acoustic branches and a stiffening in the highest frequency region due to the appearance of phonons at about 24.8 meV, localized on the $GeTe_4$ tetrahedra.[10,11,14]. Moreover, while in crystalline GeTe thermal conductivity is due to propagating phonons that can be described within the Boltzman transport equation, in the amorphous phase

the heat carriers are mostly non-propagating delocalized vibrations (diffusions)[15]. In addition, since crystalline GeTe is a degenerate p-type semiconductor, its electronic conductivity is three orders of magnitude larger than in the amorphous phase. We therefore need to consider the electronic contribution to TBR, as in the general case of metal/semicondutor interfaces.

The lattice contribution to the TBR has been obtained from non-equilibrium molecular dynamics (NEMD) simulations with the NN potential. The electronic contribution to the TBR has been computed according to the theory developed by Majumdar and Reddy[17] from phonon dispersion relations and the electron-phonon coupling constant obtained within DFT. Moreover we have computed the lattice thermal conductivity of crystalline GeTe, for which experimental data are scattered over a wide range of values 0.1-4.1 W/(mK)[18–23], possibly because of the difficulties in disentangling the lattice and electronic contributions to κ, or because of different vacancy concentrations.

II. COMPUTATIONAL METHODS

A. Molecular dynamics simulations and lattice contribution to the thermal boundary resistance

The NN interatomic potential of GeTe was obtained in Ref. 11 by fitting a large database of DFT energies using the method introduced by Behler and Parrinello[12]. The database consists of the total energies of about 30000 configurations of 64-, 96-, and 216-atom supercells computed with the Perdew-Burke-Ernzerhof exchange and correlation functional[24] and norm conserving pseudopotentials. The reliability of the DFT framework in describing structural and dynamical properties of GeTe and other phase change materials was demonstrated in several previous works[7–10]. The transferability of the NN potential was formerly validated by simulations of liquid, amorphous and crystalline GeTe[11,15,25?] . NN equilibrium molecular dynamics (MD) calculation of the thermal conductivity of bulk amorphous GeTe yields κ=0.27 ± 0.05 W/mK[15], which is very close to experimental results of 0.24 ∼ 0.25 W/mK[18,26]. The NN potential also reproduces well the structural parameters of the trigonal ferroelectric phase (space group *Rm3m*)[27] stable at normal conditions. The trigonal phase, with two atoms per unit cell, can be seen as a distorted rocksalt geometry with an elongation of the cube diagonal along the [111] direction and an off-center displacement of the inner Te atom along the [111] direction giving rise to a 3+3 coordination of Ge with three short and stronger bonds (2.84 Å) and three long and weaker (3.17 Å) bonds. In the conventional hexagonal unit cell of the trigonal phase, the structure can be also seen as an arrangement of GeTe bilayers along the c direction with shorter intrabilayer bonds and weaker interbilayers bonds (see Fig. 1).

The structural parameters of the trigonal phase consist of the lattice parameter a, the trigonal angle α, and the internal parameter x that assigns the positions of the two atoms in the unit cell, namely, Ge at (x,x,x) and Te at (-x,-x,-x)[27]. The structural parameters optimized at zero temperature with the NN potential are compared in Table I with experimental data and DFT results. The trigonal phase transforms experimentally into the cubic paraelectric phase (space group $Fm\bar{3}m$) above the Curie temperature of 705 K[28]. Although we have not estimated the theoretical thermodynamic transition temperature for the trigonal → cubic transformation, we have verified that the trigonal phase is locally stable up to 500 K in constant pressure simulations with the NN potential.

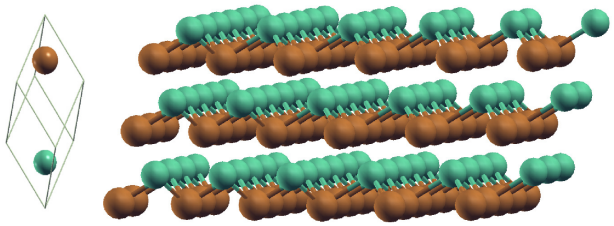

FIG. 1. IMMAGINE PROVVISORIA Geometry of the GeTe crystal seen as a stacking of bilayers along the c axis of the conventional hexagonal unit cell with the three short intrabilayers bonds and three long interbilayers bonds.

Structural parameters	DFT	NN	Exp.
a (Å)	4.33	4.47	4.31
α	58.14°	55.07°	57.9°
Volume (Å^3)	54.98	55.95	53.88
x	0.2358	0.2324	0.2366
Short, long bonds (Å)	2.85, 3.21	2.81, 3.31	2.84, 3.17

TABLE I. Structural parameters of the trigonal phase of crystalline GeTe computed with the NN potential, within DFT and from the experimental data[27]. The lengths of the short and long bonds are also given.

To study the thermal conductivity and the TBR we used the "reverse NEMD" scheme proposed by Müller-Plathe[29]. In this method, one sets up a stationary heat flux $\mathbf{q}$ between a source and a sink at two edges of the simulation cell, which gives rise to a temperature gradient in bulk materials and to a temperature jump at an interface. The bulk thermal conductivity in the linear regime κ is computed exploiting Fourier's law as $\kappa = -\mathbf{q}/\nabla T$. The Kapitza resistance R between two media at the interface sketched in Fig. 2a is defined by

$$R = \frac{T_2 - T_1}{q}$$

where q is the heat flux flowing across the interface in steady conditions and T_1 and T_2 are the temperatures in

the two media in proximity of the interface. The notations in text and figure are inconsistent. The simulations were performed with the NN code RuNNer[30] by using the DL_POLY v2.19[31] code as MD driver. The time step was set to 2 fs.

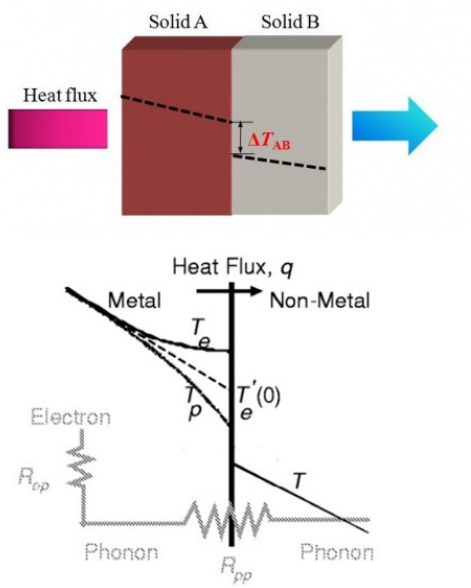

FIG. 2. IMMAGINE PROVVISORIA a) Temperature jump across the interface between two media crossed by a heat flux q. The temperature profile in the two media is schematically represented by dashed lines. b) Temperature profile of electrons (T_e) and ions T_p at the metal/non-metal interface crossed by a heat flux q according to the theory of Majumdar and Reddy[17]. $R_{pp} = \Delta T_p/q = (T_p - T)/q$ is the phonon contribution to the total thermal boundary resistance $R = (T'_e - T)/q$.

B. Electron-phonon coupling and electronic contribution to the thermal boundary resistance

The crystal/amorphos interface is a metal/non-metal junction, as the electrical conductivity of trigonal GeTe is about three orders of magnitude larger than in the amorphous phase. Heat is carried by both electrons and phonons in the crystal, but only by phonons in the amorphous phase. As a consequence at the crystalline side of the interface an energy transfer from electrons to ions takes place to allow the transfer of heat across the junction. This is possible because of the a non-equilibrium steady state is established, in which the temperature of the electrons (T_e) is higher than the temperature of the ions (T_p) as sketched in Fig. 2. Majumdar and Reddy[17] developed a theory to cope with this effect that provides an expression for the thermal boundary resistance R given by the sum of a phononic (R_{pp}) and electronic (R_e) contribution:

$$R = R_{pp} + R_e = R_{pp} + \left(\frac{1}{1+\frac{\kappa_{ph}}{\kappa_e}}\right)^{\frac{3}{2}} \sqrt{\frac{1}{G\kappa_{ph}}} \qquad (1)$$

where κ_e and κ_{ph} are the electronic and phononic contribution to the thermal conductivity of the metal and $R_{pp} = \Delta T_p/q$ (cf. Fig. 2b). The two thermal resistances are in series as electrons have to first transfer energy to the lattice to let heat transfer across the interface by phonons. R_{pp} has been computed by NEMD, as discussed above, while R_e is controlled by the parameter G, defined by $\frac{dE}{dt} = -G(T_e - T_p)$, where E is the electronic energy density and t is the time. The parameter G controls the electron to phonon energy transfer rate per unit volume, which depends on the electron-phonon coupling constant λ and on the electronic density of states (DoS) at the Fermi level $N(E_F)$ as

$$G = \pi k_B \lambda \hbar < \omega^2 > N(E_F) \qquad (2)$$

where $< \omega^2 >$ is the second moment phonon spectrum according to McMillan[32]. To compute the electron-phonon coupling constant and the G parameter we resort to DFT calculations. We used the PBE exchange-correlation energy functional[24] and norm conserving pseudopotentials, as implemented in the Quantum-Espresso suite of programs[33]. Only outermost s and p electrons were considered in the valence. The spin-orbit interaction was neglected since it has been shown to have negligible effects on the structural and vibrational properties of GeTe[34]. Kohn-Sham (KS) orbitals were expanded in a plane waves basis up to a kinetic cutoff of 30 Ry. The Brillouin Zone (BZ) integration for the self-consistent electron density was performed over a 12×12×12 Monkhorst-Pack (MP) mesh[35]. Results on the equilibrium geometry of trigonal GeTe are given in Table I.

The ideal GeTe crystal is a narrow gap semiconductor with a DFT-PBE band gap of 0.45 eV. It turns into a degenerate semiconductor because of defects in stoichiometry, in the form of Ge vacancies, which induce the formation of holes in the valence band[36]. We considered a p-doping of $8 \cdot 10^{19}$ holes/cm^3 studied experimentally in Ref.[37], and a larger hole concentration of $2.1 \cdot 10^{21}$ holes/cm^3, also investigated in previous DFT work[34]. The former and latter holes concentrations will be referred to hereafter as n_{h1} and n_{h2}. The p-doping is introduced by removing electrons and by neutralizing the system with a uniform positive background[34]. We relaxed the atoms positions at the two doping levels by keeping the lattice parameters fixed at the values of the ideal crystal: the x internal coordinate becomes 0.2359 (cf. Table 1) for both n_{h1} and n_{h2}. The Ge vacancies, present in the real crystal but lacking in our models of the p-type compound, are in fact expected to affect the lattice parameters, as much as the holes in the valence bands do[34].

Phonon dispersion relations were calculated using density functional perturbation theory (DFPT)[38] for both

the ideal crystal and the two p-dopings, computing the dynamical matrices on a 6×6×6 uniform mesh in the BZ.

The electron-phonon coupling constant λ was computed as

$$\lambda = 2\int_0^\infty \frac{\alpha^2F(\omega)}{\omega}d\omega \quad (3)$$

where $\alpha^2F(\omega)$ is the Eliashberg spectral function which measures the contribution of phonons with frequency ω to the electron-phonon coupling:

$$\alpha^2F(\omega) = \frac{2}{\hbar N(E_F)}\sum_{\vec{q},\nu}\delta(\omega-\omega_{\vec{q},\nu})\times$$
$$\sum_{\vec{k},n,m}\delta(\epsilon_{\vec{k},n}-E_F)\mid g^{n,m}(\vec{k}\vec{q}\nu)\mid^2\delta(\epsilon_{\vec{k}+\vec{q},m}-E_F) \quad (4)$$

where the first sum runs over phonon bands at frequency $\omega_{\vec{q},\nu}$ while in the second sum the index n,m runs over electronic states at energies $\epsilon_{\vec{k},n}$ and $\epsilon_{\vec{k}+\vec{q},m}$. $N(E_F)$ is the electronic density of states of both spins per cell at the Fermi energy E_F and $g^{n,m}(\vec{k}\vec{q}\nu)$ is the electron-phonon matrix element. This is given in turn by

$$g^{n,m}(\vec{k}\vec{q}\nu) = \sqrt{\frac{\hbar}{2\omega_{\mathbf{q},\nu}}}\langle u_{\mathbf{k}+\mathbf{q},m}\mid \mathbf{M}^{-\frac{1}{2}}\nabla V^{\mathbf{q}}_{\text{eff}}\epsilon_{\nu\mathbf{q}}\mid u_{\mathbf{k},n}\rangle \quad (5)$$

where $\mathbf{M}$ is the atomic mass matrix, $u_{\mathbf{k},n}$ is the periodic part of the Kohn-Sham state, $\epsilon_{\nu\mathbf{q}}$ is the normalized eigenstate of the dynamical matrix, and $\nabla V^{\mathbf{q}}_{\text{eff}}$ is the derivative of the Kohn-Sham effective potential with respect to the atomic displacement caused by a phonon with wavevector $\mathbf{q}$. The two δ functions containing the electron band energies were replaced by order-one Hermite-Gauss smearing function with different value of variance ranging from 0.0005 to 0.05 Ry[39]. The second moment phonon spectrum $<\omega^2>$ according to McMillan[32] is given in turn by

$$<\omega^2> = \frac{\int\omega\alpha^2F(\omega)d\omega}{\int\frac{\alpha^2F(\omega)d\omega}{\omega}} \quad (6)$$

The electron-phonon matrix elements are computed by means of DFPT on a 6x6x6 q-point grid for the phonons and on a dense 132x132x132 k-points grid for n_{h1} and 96x96x96 k-point grid for n_{h2} for the electrons. Most of the variation of the value of λ with the size of k and q-point mesh can be ascribed to fluctuations in the density of states at the Fermi level. The quantity $\alpha^2F(\omega)/N(E_F)$ thus converges faster with the size of k and q-point mesh[40]. Then the value of λ is obtained by multiplying $\lambda/N(E_F)$ by a more accurate value of $N(E_F)$ computed using the tetrahedron method over a uniform 160x160x160 k-point mesh. We estimated a total error in λ below 10%. Convergence with respect to the smearing is shown in Fig. 10 in the Appendix.

III. RESULTS

A. Phonons and electron-phonon coupling in crystalline GeTe from DFT calculations

The phonon dispersion relations of GeTe along high symmetry direction in the BZ are reported in Fig. 3 for both stoichiometric and hole-doped GeTe. The results are very similar to those reported in Ref.[34], computed with DFT-LDA. As usual, phonons are somehow softer with PBE than with LDA functional. The metallic character of the hole-doped systems removes the discontinuities in the phonon dispersion at the Γ point (TO-LO splitting) present in the stoichiometric compound. The highest frequency phonon of A_1 symmetry (at Γ) softens continuously by increasing p-doping as already shown in Ref.[34]. The A_1 mode, measured experimentally by Raman spectroscopy[41], shows a strong temperature dependance as it corresponds to the soft mode of the ferroelectric transition. The experimental frequency extrapolated to zero temperature is 17.4 meV in the sample measured in Ref.[41], for which the doping level is unknown. The theoretical frequency is 18.6 meV in the stoichiometric compound and 14.9 meV in the system with $n_{h2}=2.1\cdot10^{21}h/cm^3$, which means that we could match the experimental frequency by a suitable choice of doping.

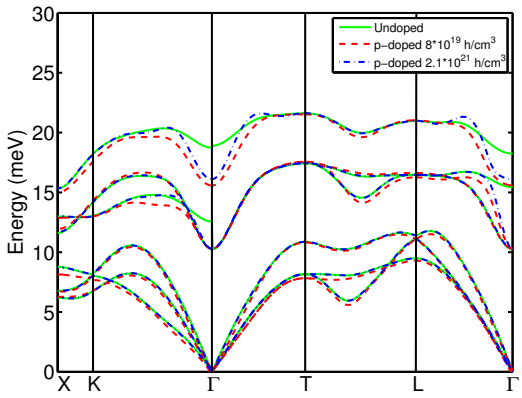

FIG. 3. Phonon dispersion relation of GeTe. The continuous line refers to the results for the stoichiometric compound while the dashed line correspond to the p-doped system with $n_h=8\cdot10^{19}$ holes/cm^3 and the dot-dashed line to $n_h=2.1\cdot10^{21}$ holes/cm^3. (La frequenza del LO a Gamma non e' monotona decrescente col doping: sei sicuro che rosso e blu non siano scambiati? La riga verde lungo Γ-T non si vede: puoi farla piu' spessa?)

The Eliashberg function and the phonon density of states are reported in Figs. 4,5 for the two doping levels. The electronic density of states (DOS) does not depend on the holes concentration in the range of n_h considered here as shown in Fig. 6. The average phonon frequency according to Eq. 6 is $(<\omega^2>)^{\frac{1}{2}}=13.05$ meV for $n_{h1}=8\cdot10^{19}h/cm^3$ and $(<\omega^2>)^{\frac{1}{2}}=10.79$ meV for

n_{h2}. The band structure along high symmetry direction of the BZ close to the energy gap and the electronic density of states are reported in Fig. 6. An increase in n_h simply shifts the Fermi level deeper in the valence band with no significant changes in the DOS. Integration of $\alpha^2F(\omega)$ leads to very similar values of $\lambda/N(E_F)$ for the two doping levels, namely 0.12 (1/states/Ry/unit cell) for both n_{h1} and n_{h2}. The DoS at the Fermi level is in turn 0.64 states/Ry/cell and 4.3 states/Ry/cell, which yields λ=0.077 for n_{h1} and λ=0.51 for n_{h2}. Since $\lambda/N(E_F)$ is poorly dependent of the hole concentration, it is possible to estimate the value of λ at different doping levels by multiplying our result for $\lambda/N(E_F)$ with the actual density of state at the Fermi level.

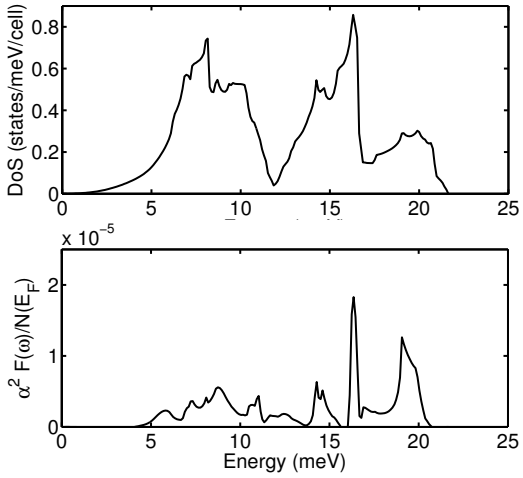

FIG. 4. Phonon density of states and Eliashberg function $\alpha^2F(\omega)/N(E_F)$ for GeTe with holes concentrations of n_{h1}=8$\cdot$ 10^{19} holes/cm^3.

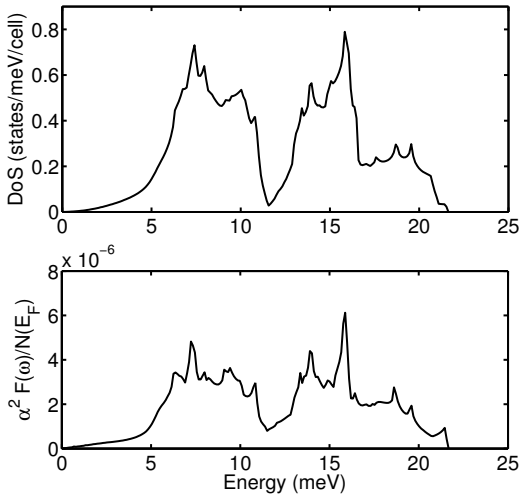

FIG. 5. Phonon density of states and Eliashberg function $\alpha^2F(\omega)/N(E_F)$ for GeTe with holes concentrations of n_{h2}=2.1 $\cdot$ 10^{21} holes/cm^3.

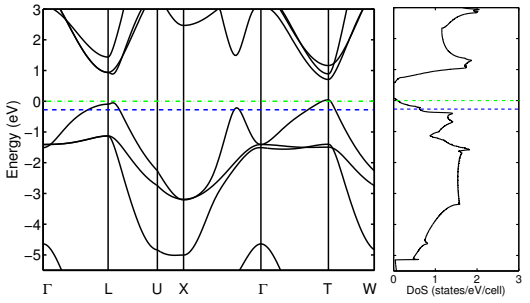

FIG. 6. Electronic bands along high symmetry directions and electronic density of states (DoS) of trigonal GeTe. The DoS does not change by hole doping on the scale of the figure. The position of the Fermi level is indicated by a dot-dashed line (dashed line) for hole concentration n_{h1}=8 $\cdot$ 10^{19} holes/cm^3 (n_{h2}=2.1 $\cdot$ 10^{21} holes/cm^3). The DoS are computed with the tetrahedron method on a 160x160x160 mesh and aligned at the lowest energy.

B. Electronic contribution to the thermal boundary resistance

The parameter G (Eq. 2) has been computed for the two representative hole concentrations n_{h1}=8 $\cdot$ 10^{19} holes/cm^3 and n_{h2}= 2.1 $\cdot$ 10^{21} holes/cm^3 (cf.[34,37]) from the electron-phonon coupling constant and $\langle\omega^2\rangle$ discussed in the previous section. The values of G is 1.43 $\cdot$ 10^{15} W/(m^3 K) for n_{h1} and 4.5 $\cdot$ 10^{16} W/(m^3 K) for n_{h2} . By using the phononic thermal conductivity $\kappa_{ph} \sim 3.1$ W/(m K) as calculated in Sec. IIID, the ratio κ_e/κ can be chosen such that the prefactor in R$_e$ (cf. Eq. 1) is in the range $0.086 < (\kappa_e/\kappa)^{\frac{3}{2}} < 1$ where the lower extreme corresponds to the low value of κ_e=0.73 W/(mK) for the sample measured in Ref.[18]. (this part is quite unclear: what is the prefactor of R$_e$ in Eq.1? try to be more explicit.) By plugging these numbers into formula 1, R_e falls in the range 1.3 $\cdot$ 10^{-9}-1.4 $\cdot$ 10^{-8} m^{2}K/W for n_{h1} and 2.2 $\cdot$ 10^{-10}-2.6 $\cdot$ 10^{-9} m^{2}K/W for n_{h2}.

Note that the sample with holes density n_{h1}= 8 $\cdot$ 10^{19} holes/cm^3 measured in Ref.[37] displays an electrical resistivity of ρ=1.4 $\cdot$ 10^{-4} Ω cm while in a more recent work[42] Hall measurements on samples with the same resistivity of about ρ=1.4 $\cdot$ 10^{-4} Ω cm yielded a much higher holes concentration of 8 $\cdot$ 10^{20} holes/cm^3 possibly because of a different hole mobility. The estimate of R_e for a specific sample thus requires the measurements of both n_h (or $N(E_F)$ by whatever means) and κ_e eventually from ρ and the application of the Wiedemann-Franz law. For the specific sample of Ref.[37] for which both n_h (8 $\cdot$ 10^{19} holes/cm^3) and ρ (1.4 $\cdot$ 10^{-4} Ω) (ρ si misura in Ωm) are known we can estimate κ_e=5.22 W/m$\cdot$ K from the Lorenz number L_o= 2.44 $\cdot$ 10^{-8} WΩ/K and κ_e=L_oT/ρ for T=300 K, which finally yields R$_e$= 0.7 $\cdot$ 10^{-8} K m^2/W. This value is actually larger than the lattice contribution as we will see in the next sections.

The calculated value of G can be used to estimate R$_e$ also for the interface of GeTe with other dielectrics.

C. Lattice thermal conductivity of bulk amorphous GeTe

The amorphous models were generated by quenching from the melt (1000 K) to 300 K in 100 ps, according to the protocol used in our previous works[11,15]. We considered several supercells with different size, up to 24.8 Å x 24.8 Å x 397.3 Å (8192 atoms). The heat source and sink are placed at the edges of the cell along the z-direction, they consists of a slice of mobile atoms 5 Å thick along z neighboring a region of fixed atoms, which decouple the source and the sink in the presence of periodic boundary conditions (see Fig. 7).

A plot of the temperature profile in the largest simulation cell is shown in Fig. 7. The temperature profile reaches a converged steady condition after 800 ps. The temperature of the sink and source are ? K and ? K and the imposed flux is q=?. From the Fourier law q=-$\kappa\frac{dT}{dz}$ and the slope of the temperature profile we obtain κ=0.26 W/(mK) which is very close to our previous result of 0.27±W/(mK) at 300 K obtained from equilibrium MD and the use of the Green-Kubo formula[15]. We checked the convergence of κ by using supercells with different cross section areas perpendicular to the heat flux, and with different length along z. We probed the thermal conductivity for a cross-section areas of 24.8 x 24.8 Å^2 and 49.7 x 49.7 Å^2. Since the phonon mean free path in a-GeTe is always below few Å[15], κ is already converged in a smaller 24.8 Å x 24.8 Å x 99.3 Å (2048 atoms) cell. Since the phononic specific heat has already reached its classical limit at 300 K, possible changes of κ with temperature should arise only from the increase of anharmonicities at higher temperatures. (agree, but what is the point to mention it here?)

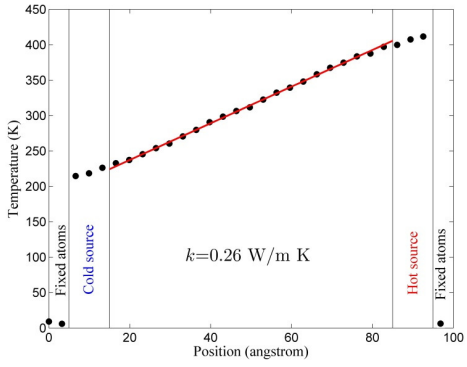

FIG. 7. IMMAGINE PROVVISIORIA Temperature profile in the NEMD simulation of bulk amorphous GeTe under a steady state heat flux q=?.

We also investigated possible non-linear effect by tuning the initial temperature and the heat flux in order to have large temperature gradients from 1 K/nm up to a value of 30 K/nm which might arise in PCM during the reset process. We actually did not observe changes of κ within the error bar of 0.03 W/(mK) for $\frac{dT}{dz}$ in the range given above and for an average temperature in the range 200-400 K at which the amorphous phase is stable against crystallization on the time scale of our simulations. We can conclude at the conditions of the PCM operation we can still use the bulk value of the thermal conductivity of a-GeTe measured/computed for small temperature gradients.

D. Lattice thermal conductivity of bulk crystalline GeTe

In a trigonal crystal one expect different values of the thermal conductivity along the z direction (c axis of the conventional hexagonal cell) and in the xy plane. The values of κ_z and κ_x were computed within NEMD by setting the planes of the sink and sources either perpendicular to the z direction or to the x direction in supercells of the trigonal phase at the theoretical lattice parameters optimized at zero temperature (cf. Sec. II).

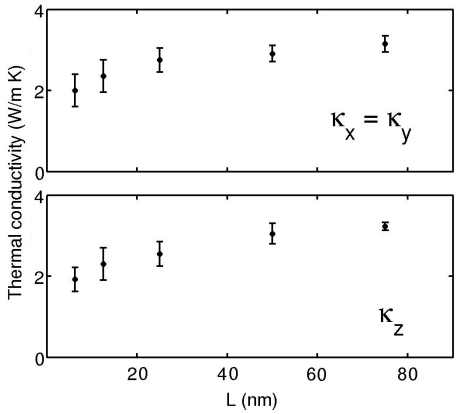

FIG. 8. The dependence of the thermal conductivity κ as a function of the size of the simulation cell L long for the trigonal crystalline phase. The thermal conductivity perpendicular (parallel) to the c-axis is reported in the upper (lower) panel.

In particular κ_z is obtained with supercells with sizes from 28.6 Å x 24.8 Å x 56.71 Å to 28.6 Å x 24.8 Å x 748.61 Å where the longer edges are along the c direction of the conventional hexagonal cell while $\kappa_x = \kappa_y$ is obtained with sizes from 21.5 Å x 22.7 Å x 62.0 up to 21.5 Å x 22.7 Å x 744.1 Å. The dependance of κ on L is reported in Fig. 8. We obtained a converged value κ_z= 3.23 ± 0.1 W/(mK) and $\kappa_x = \kappa_y$ =3.15 ± 0.2 W/(mK).

For a polycrystalline sample the calculated effective thermal conductivity κ_{eff}=$\frac{2}{3}\kappa_x + \frac{1}{3}\kappa_z$=3.2 W/(mK) which is comparable, although larger, than the experimental value of 2.35 ± 0.53 W/(mK) of Ref.[18]. Our result thus confirm a sizable contribution of the lattice to the thermal conductivity of trigonal GeTe in agreement with the most recent experimental data of Ref.[18] but in

contrast to the conclusions of previous experimental work in Ref.[21].

A better agreement with experiments is actually obtained by including the effect of Ge vacancies on the thermal conductivity. Ge vacancies are expected to be present in the real material, with concentration depending on preparation conditions up to a few %. The vacancies generate holes in the valence band which turn the stoichiometric narrow gap compound in a degenerate p-type semiconductor[36]. We introduced vacancies in a random manner on the Ge sublattice with concentration of 3 % corresponding to the hole concentration of $1.1{\cdot}10^{21}$ holes/cm^3 (two holes per vacancy). We then repeated the simulations with vacancies and a 28.6 Å x 24.8 Å x 499.0 Å supercell yielding κ_z=1.55 ± 0.1 W/(mK) which 49% lower than the value obtained with the same supercell at the same average temperature of 300 K for the stoichiometric compound. Similarly we obtained $\kappa_x = \kappa_y$=1.3 ± 0.2 W/(mK) with the supercell of size 21.5 Å x 22.7 Å x 496.0 which is 56% lower than the value for the stoichiometric compound at the same conditions. We can thus conclude that vacancies with concentration up to 3% can significantly reduce the thermal conductivity in agreement with the experimental data of Ref.[23]. This also leads to an enhancement of the electronic contribution to the thermal boundary resistance R$_e$ by about $\sqrt{2}$.

E. Lattice contribution to the thermal boundary resistance at the crystal-amorphous interface

We computed the lattice contribution R_{pp} to the TBR by performing NEMD simulations in supercells made of the junction of the amorphous and crystalline models discussed in Secs. IIIa-b above. We considered two interfaces, one lying on the (111) crystalline plane and a second in the (100) crystalline plane in the rhombohedral notation for the GeTe crystal. For the (111) interface we used a supercell with edges 50.1 Å x 49.6 Å x 348.5 Å made by a junction between a 28.6 Å x 24.8 Å x 249.5 Å cell of the bulk crystal and a 28.6 Å x 24.8 Å x 99.3 Å cell of the bulk amorphous phase. The length along the z direction of the amorphous and crystalline regions is comparable to the typical size of an ultrascaled PCM device. The supercell was then annealed at 500 K for 20 ps and then quenched again at 300 K in 20 ps to optimize the interface geometry.

The steady temperature profile reached in about 2.2 ns of simulation is shown in Fig. 9. The stoichiometric trigonal phase is considered.

A temperature jump at the interface can not be appreciated in Fig. 9. If any it is smaller than the size of temperature fluctuations still present in the model due to the finite simulation time. Note that to achieve convergence in the temperature profile a much longer simulation time is needed in the presence of an interface with respect to the homogeneous bulk models. We repeated the simulations for the (100) interface with similar results. We can thus set an upper limit to R_{pp} for both interfaces of about $2{\cdot}\ 10^{-9}$ m^{2}K/W which is comparable to the electronic contribution discussed in Sec. IIIB. In fact, the lattice contribution is lower than the electronic contribution ($0.7 \cdot 10^{-8}$ m^{2}K/W) to the TBR for the hole concentration and electronic conductivity of the sample of Ref.[37].

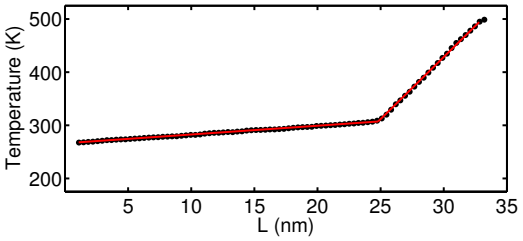

FIG. 9. Temperature profile in the NEMD simulation of the junction between the amorphous and crystalline phases. The heat sink and source are separated by 330 Å. The interface lies on the (111) crystalline plane. The heat flux is q=9.8 kJ/mol/ps.

IV. CONCLUSIONS

We have computed phonon dispersion relations and the electron-phonon coupling constant λ for the phase change compound GeTe at different levels of p-doping which, in the real system, is due to the presence of Ge vacancies. The quantity $\lambda/N(E_F)$ is slightly dependent on the p-doping for hole concentration in the range $8{\cdot}10^{19}$-$2.1{\cdot}10^{21}$ holes/cm^3 which correspond to a vacancy concentrations in the range 0.2-5.7 %. The calculated λ allowed us to estimate the electron-phonon contribution R_e to the thermal boundary resistance (TBR) at the interface between the trigonal crystal and the amorphous phase which is present in the memory device. This contribution, calculated according to the theory of Majumdar and Reddy[17], is dependent on the concentration of vacancies via the density of states $N(E_F)$ and on hole mobility which leads to large fluctuations of R_e in the range 10^{-8}-10^{-10} m^{2}K/W. For a specific system for which both the hole concentration and the electronic conductivity is known (Ref.[37]) the electronic contribution to the TBR ($0.7 \cdot 10^{-8}$ m^{2}K/W) is larger than the upper bound ($2 \cdot 10^{-9}$ m^{2}K/W) that we have estimated for the lattice contribution to the TBR from non-equilibrium molecular dynamics simulations. NEMD simulations of the bulk thermal conductivity of crystalline GeTe also reveal that the presence of about 3 % of Ge vacancies reduce the lattice thermal conductivity from 3.1 W/(mK) to 1.2 W/(mK) which justifies the large spread in the thermal conductivity measured experimentally.

ACKNOWLEDGMENTS

We acknowledge funding from the European Union Seventh Framework Programme FP7/2007-2013 under grant agreement No. 310339 and computational resources provided by Cineca (Casalecchio di Reno, Italy) through program ISCRA.

V. APPENDIX

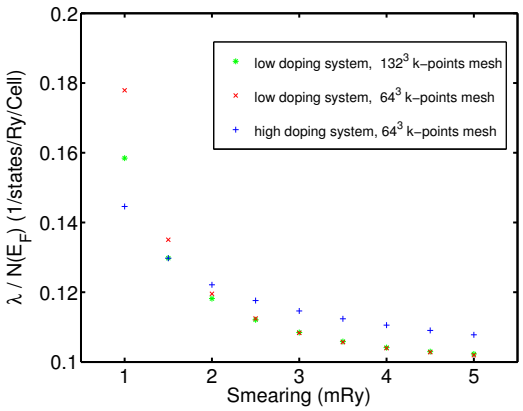

FIG. 10. Dependence of the electron-phonon coupling constant $\lambda/N(E_F)$ on the smearing parameter (eV) of the Dirac δ-functions in Eq. 4. The doping of $8 \cdot 10^{19}$ hole/cm^3.

* corresponding author: marco.bernasconi@mater.unimib.it

[1] M. Wuttig and N. Yamada, Nat. Mater. **6**, 824 (2007).
[2] A. Pirovano, A. L. Lacaita, A. Benvenuti, F. Pellizzer, and R. Bez, IEEE Trans. Electron. Dev. **51**, 452 (2004).
[3] A.L. Lacaita and D.J. Wouters, Phys. Stat. Sol. A **205**, 2281 (2008).
[4] D. Lencer, M. Salinga, and M. Wuttig, Adv. Mat. **23**, 2030 (2011).
[5] S. Raoux, W. Welnic, and D. Ielmini, Chem. Rev. **110**, 240 (2010).
[6] J. P. Reifenberg, D. L. Kencke, and K. E. Goodson, IEEE Elec. Dev. Lett. **29**, 1112 (2008).
[7] S. Caravati, M. Bernasconi, T. D. Kühne, M. Krack, and M. Parrinello, Appl. Phys. Lett. **91**, 171906 (2007).
[8] J. Akola and R. O. Jones, Phys. Rev. B **76**, 235201 (2007).
[9] J. Hegedüs and S. R. Elliott, Nat. Mater. **7**, 399 (2008).
[10] R. Mazzarello, S. Caravati, S. Angioletti-Uberti, M. Bernasconi, and M. Parrinello, Phys. Rev. Lett.
[11] G. C. Sosso, G. Miceli, S. Caravati, J. Behler, and M. Bernasconi, Phys. Rev. B **85**, 174103 (2012).
[12] J. Behler, and M. Parrinello, Phys. Rev. Lett. **98**, 146401 (2007); J. Behler, J. Chem. Phys. **134**, 074106 (2011).
[13] L. Perniola, *et al.*, IEEE Elect. Dev. Lett. **31**, 488 (2010).
[14] T. Matsunaga *et al.*, Adv. Mat. **21**, 2232 (2011).
[15] G. C. Sosso, D. Donadio, S. Caravati, J. Behler, and M. Bernasconi, Phys. Rev. B **86**, 104301 (2012).
[16] G. C. Sosso, G. Miceli, S. Caravati, J. Behler, and M. Bernasconi, J. Phys. Chem. Lett. **4**, 4241 (2013).
[17] A. Majumdar and P. Reddy, Appl. Phys. Lett. **84**, 4768 (2004).
[18] R. Fallica, E. Varesi, L. Fumagalli, S. Spadoni, and M. Longo, Physica Status Solidi RRL (2013). B **52**, 16321 (1995).
[19] L. E. Shelimova, O. G. Karpinskii, P. P. Konstantinov, M. A. Kretova, E. S. Avilov, and V. S. Zemskov, Inorg. Mat. **37**, 421 (2001).
[20] P. Nath and K. L. Chopra, Phys. Rev. B **10**, 3412 (1974).
[21] R. Lan, R. Endo, M. Kuwahara, Y. Kobayashi, and M. Susa, J. Appl. Phys. **112**, 053712 (2012).
[22] J. M. Yanez-Limon, J. Gonzalez-Hernandez, J. J. Alvarado-Gil, I. Delgadillo, and H. Vargas, Phys. Rev. B **52**, 16321 (1995).
[23] D. H. Damon, M. S. Lubell, and R. Mazelsky, J. Phys. Chem. Solids **28**, 520 (1967).
[24] J. P. Perdew, K. Burke and M. Ernzerhof, Phys. Rev. Lett. **77**, 3865 (1996).
[25] G. C. Sosso, J. Behler, and M. Bernasconi, Physica Status Solidi B **249**, 1880 (2012).
[26] J. P. Reifenberg, M. A. Panzer, S. Kim, A. M. Gibby, Y. Zhang, S. Wong, H.-S. P. Wong, E. Pop, K. E. Goodson, Appl. Phys. Lett. **91**, 111904 (2007).

[27] J. Goldak, C.S. Barrett, D. Innes, and W. Youdelis, J. Chem. Phys. **44**, 3323 (1966).
[28] T. Chattopadhyay, J. Boucherle, and H. Von Schnering, J. Phys. C **20**, 1431 (1987).
[29] F. Muller-Plathe, J. Chem. Phys. **106**, 6082 (1997).
[30] RuNNer: A Neural Network Code for High-Dimensional Potential-Energy Surfaces, Jörg Behler, Lehrstuhl für Theoretische Chemie, Ruhr-Universität Bochum, Germany.
[31] W. Smith and T. R. Forester, J. Mol. Graph. **14**, 136 (1996).
[32] P. B. Allen, Phys. Rev. Lett. **59**, 1460 (1987).
[33] P. Giannozzi et al., J.Phys.:Condens.Matter, **21**, 395502 (2009); www.quantum-espresso.org.
[34] R. Shaltaf, X. Gonze, M. Cardona, et al., Phys. Rev. B **79**, 075204 (2009).
[35] H. Monkhorst, and J. D. Pack, Phys. Rev. B **13**, 5188 (1976).
[36] A. H. Edwards, A. C. Pineda, P. A. Schultz, M. G. Martin, A. P. Thompson, H. P. Hjalmarson, and C. J. Umrigar, Phys. Rev. B **73**, 045210 (2006).
[37] A. J. Bevolo, H. R. Shanks, and D. E. Eckels, Phys. Rev. B **13**, 3523 (1976).
[38] S. Baroni, S. de Gironcoli, and A. Dal Corso, Rev. Mod. Phys. **73**, 515 (2001).
[39] M. Methfessel and A. T. Paxton, Phys. Rev. B **40**, 3616 (1989).
[40] I. Spagnolatti, M. Bernasconi, and G. Benedek, Europhys. Lett. **59** 572-578 (2002).
[41] E.F. Steigmeier and G. Harbeke, Solid State Comm. **8**, 1275 (1970).
[42] E. M. Levin et al. J. Appl. Phys. **114**, 083713 (2013)